Angewandte Chemie
Eine Zeitschrift der Gesellschaft Deutscher Chemiker

Supporting Information

# Mixed Metal–Organic Framework with Multiple Binding Sites for Efficient $C_2H_2/CO_2$ Separation

*Junkuo Gao,* Xuefeng Qian, Rui-Biao Lin,* Rajamani Krishna, Hui Wu, Wei Zhou,* and Banglin Chen**

anie_202000323_sm_miscellaneous_information.pdf

## 1. Materials and general methods

All chemicals were purchased from Alfa Aesar, TCI chemical and Aldrich and used without further purification. Powder X-ray diffraction data were recorded on a Bruker D8 Advance diffractometer with a graphite-monochromatized Cu Ka radiation. The gas sorption isotherms were collected using an automatic volumetric adsorption apparatus Micromeritics ASAP 2020. The specific surface areas of sample were measured with a $N_2$ adsorption-desorption isotherms by the Brunauer-Emmett-Teller (BET) method at 77 K. All the samples were degassed at 100 ℃ for 3 hours before the gas sorption measurements. Thermogravimetric analysis (TGA) was carried out under air atmosphere from room temperature to 500 °C using a Shimadzu TGA-50 analyzer at a heating rate of 10 °C $min^{-1}$. For variable-temperature powder X-ray diffraction (VT-PXRD), the measured parameter included a scan speed of 10 º $min^{-1}$, a step size of 0.02º and a scan range of 2θ from 10º to 40º. The heating rate is 5 ℃ $min^{-1}$ and the sample was maintained 5 minutes at each target temperature. The target temperatures are set as follows: 60 ℃, 90 ℃, 120 ℃, 150 ℃, 180 ℃ and 200 ℃. The energy-dispersive X-ray spectroscopy (EDS) analyses were carried out by transmission electron microscopy (TEM, JEM-2100).

## 2. Synthesis of [Fe(pyz)Ni(CN)$_4$] (FeM-M'MOF)

$Fe(ClO_4)_2 \cdot xH_2O$ (1 mmol) and pyrazine (1 mmol) were dissolved in a mixture of 50 ml of deionized water and 50 ml of methanol under the protection of $N_2$. **Caution! Iron (II) perchlorate salt is potentially explosive and must be handled with care!** Separately, 1 mmol of $K_2[M(CN)_4]$ (M = Ni, Pt) is dissolved in 20 ml of deionized water and the solution is dropwise added to the $Fe(ClO_4)_2 \cdot xH_2O$-pyrazine solution. Precipitation of the clathrates instantaneously occurs under vigorous stirring. After stirring for 30 minutes, separated by Centrifuge the powder was recovered and washed with water several times, then dry in vacuum overnight at room temperature. Elemental analysis of activated **FeNi-M'MOF** ($C_8H_4N_6FeNi$), Calcd: C. 32.17%; H, 1.35%; N, 28.14% and found: C, 32.45%; H, 1.64%; N, 28.36%.

## 3. Fitting of pure component isotherms

The experimentally measured loadings for $C_2H_2$, and $CO_2$ at 273 K, and 298 K in **FeM-M'MOF** were fitted with the dual-Langmuir isotherm model

$$q = q_{A,sat}\frac{b_A p}{1+b_A p} + q_{B,sat}\frac{b_B p}{1+b_B p} \quad (1)$$

The Langmuir parameters for each site is temperature-dependent

$$b_A = b_{A0}\exp\left(\frac{E_A}{RT}\right); \quad b_b = b_{B0}\exp\left(\frac{E_B}{RT}\right) \quad (2)$$

The Dual-site Langmuir fit parameters are provided in Table S3 and S4.

## 4. Isosteric heat of adsorption

The binding energy of $C_2H_2$ is reflected in the isosteric heat of adsorption, $Q_{st}$, defined as

$$Q_{st} = RT^2\left(\frac{\partial \ln p}{\partial T}\right)_q \quad (3)$$

## 5. IAST calculations of adsorption selectivities

In order to compare the $C_2H_2/CO_2$ separation performance of various MOFs, IAST calculations of mixture adsorption were performed. For separation of a binary mixture of components A and B, the adsorption selectivity is defined by

$$S_{ads} = \frac{q_A/q_B}{y_A/y_B} \quad (4)$$

where the $q_A$, and $q_B$ represent the molar loadings, expressed in mol $kg^{-1}$, within the MOF that is in equilibrium with a bulk fluid mixture with mole fractions $y_A$, and $y_B = 1 - y_A$. The molar loadings, also called *gravimetric uptake capacities,* are usually expressed with the units mol $kg^{-1}$. The IAST calculations of 50/50 mixture adsorption taking the mole fractions $y_A = 0.5$ and $y_B = 1 - y_A = 0.5$ for a range of pressures up to 100 kPa and 298 K were performed.

## 6. Transient breakthrough simulations

The performance of industrial fixed bed adsorbers is dictated by a combination of adsorption selectivity and uptake capacity. For a proper comparison of various MOFs, we perform transient breakthrough simulations using the simulation methodology described in the literature.[S1] or the breakthrough simulations, the following parameter values were used: length of packed bed, $L$ = 0.3 m; voidage of packed bed, $\varepsilon = 0.4$; superficial gas velocity at inlet, $u = 0.04$ m/s. The transient

breakthrough simulation results are presented in terms of a *dimensionless* time, $\tau$, defined as $\tau = \frac{tu}{\varepsilon L}$.

During the initial transience, the effluent gas contains pure $CO_2$ and this continues until $C_2H_2$ starts breaking through because its uptake capacity in the MOF has been reached.

During a certain time interval, $\Delta\tau$, pure $CO_2$ can be recovered in the gas phase. As in previous works,[S1a] we set the purity of $CO_2$ to 99.95%. The MOFs are all compared on the basis of the moles of 99.95% pure $CO_2$ produced per L of adsorbent material.

If $\tau_{break}$ is the breakthrough time for $C_2H_2$, during the time interval 0 to $\tau_{break}$, $C_2H_2$ is captured. The volumetric $C_2H_2$ capture capacity, expressed in mol/L, can be determined from a material balance.

## 7. Neutron diffraction experiment

Neutron powder diffraction (NPD) measurements were conducted using the BT-1 neutron powder diffractometer at the National Institute of Standards and Technology (NIST) Center for Neutron Research. A Ge(311) monochromator with a 75° take-off angle, $\lambda$ = 2.0787(2) Å, and in-pile collimation of 60 minutes of *arc* was used. Data were collected over the range of 1.3-166.3° (2θ) with a step size of 0.05°. Fully activated **FeNi-M'MOF** sample was loaded in a vanadium can equipped with a capillary gas line. A closed-cycle He refrigerator was used to control the sample temperature. The bare MOF sample was measured first. To investigate the gas adsorption structure, the sample was charged with gas molecules at pre-determined pressures and temperatures, and allowed enough time to reach equilibrium. Diffraction data were then collected on the gas-loaded samples. For comparison purpose, both $CO_2$ and $C_2D_2$ were studied. Note that for acetylene adsorption, deuterated gas $C_2D_2$ was used to avoid the large incoherent neutron scattering background that would be produced by the hydrogen in $C_2H_2$. Rietveld structural refinement was performed on the neutron diffraction data using the GSAS package. Due to the large number of atoms in the crystal unit cell, the ligand molecule and the gas molecule were both treated as rigid bodies in the Rietveld refinement (to limit the number of variables), with the molecule orientation and center of mass freely refined. Final refinement on lattice parameters, atomic coordinates, positions/orientations of the rigid bodies, thermal factors, gas molecule occupancies, background, and profiles all converge with satisfactory R-factors.

## 8. Breakthrough experiments

The breakthrough experiments were carried out in dynamic gas breakthrough set-up. A stainless-steel column with inner dimensions of 4 × 150 mm was used for sample packing. MOF particles (0.560 g) with size of 220-320 μm obtained through particle size sieving was then packed into the column. The column was placed in a temperature-controlled environment (maintained at 298 K). The mixed gas flow and pressure were controlled by using a pressure controller valve and a mass flow controller (Figure S1). Outlet effluent from the column was continuously monitored using gas chromatography (GC-2014, SHIMADZU) with a thermal conductivity detector (TCD, detection limit 0.1 ppm). The column packed with sample was firstly purged with He flow (100 mL $min^{-1}$) for 6 h at room temperature 298 K. The mixed gas flow rate during breakthrough process is 2 mL $min^{-1}$ using 50/50 (v/v) $C_2H_2/CO_2$. After the breakthrough experiment, the sample was regenerated under vacuum.

The actual $C_2H_2$ capture amount and separation factor of $C_2H_2/CO_2$ were calculated by reported method.[S2] The actual adsorbed amount of gas *i* ($q_i$) is calculated from the breakthrough curve by the equation:

$$q_i = \frac{F_i \times t_0 - V_{dead} - \int_0^{t_0} F_e \Delta t}{m} \quad (5)$$

where $F_i$ is the influent flow rate of the specific gas (ml $min^{-1}$); $t_0$ is the adsorption time (min); $V_{dead}$ is the dead volume of the system ($cm^3$); $F_e$ is the effluent flow rate of the specific gas (ml $min^{-1}$); and *m* is the mass of the sorbent (g). The separation factor (α) of the breakthrough experiment is determined as

$$\alpha = \frac{q_1}{q_2} \times \frac{y_2}{y_1} \quad (6)$$

where $y_i$ is the molar fraction of gas *i* in the gas mixture.

In this case, the adsorbed amounts of $C_2H_2$ are calculated to be 4.10 mol $L^{-1}$. Accordingly, the separation factor is α = 1.7.

**Table S1.** Crystallographic Data of **FeNi-M'MOF**, **FeNi-M'MOF⊃$C_2D_2$** and **FeNi-M'MOF⊃$CO_2$**.

| Compound name | **FeNi-M'MOF** | **FeNi-M'MOF⊃$C_2D_2$** | **FeNi-M'MOF⊃$CO_2$** |
|---|---|---|---|
| CCDC | 1958795 | 1958796 | 1958797 |
| Empirical formula | $C_8H_4N_6FeNi$ | $C_{9.39}H_4D_{1.39}N_6FeNi$ | $C_{8.71}H_4N_6O_{1.41}FeNi$ |
| Formula weight | 298.70 | 318.16 | 329.81 |
| Crystal system | Tetragonal | Tetragonal | Tetragonal |
| Space group | P4/mmm | P 4/mmm | P4/mmm |
| *a* (Å) | 7.1535(10) | 7.1038(9) | 7.1590(10) |
| *b* (Å) | 7.1535 | 7.1038 | 7.159 |
| *c* (Å) | 7.0515(16) | 6.9381(16) | 7.0440(14) |
| $\alpha$ (°) | 90 | 90.0 | 90.0 |
| $\beta$ (°) | 90 | 90.0 | 90.0 |
| $\gamma$ (°) | 90 | 90.0 | 90.0 |
| Volume (Å$^3$) | 360.843 | 350.124 | 361.014 |
| *Z* | 1 | 1 | 1 |
| $R_p{}^a I>2\Theta$ | 0.0195 | 0.0169 | 0.0179 |
| $R_{wp}{}^b I>2\Theta$ | 0.0242 | 0.0208 | 0.0220 |

$^aR_p = \Sigma|cY^{sim}(2\theta_i) - I^{exp}(2\theta_i) + Y^{back}(2\theta_i)|/\Sigma|I^{exp}(2\theta_i)|$.

$^bR_{wp} = \{w_p[cY^{sim}(2\theta_i) - I^{exp}(2\theta_i) + Y^{back}(2\theta_i)]2/\Sigma w_p[I^{exp}(2\theta_i)]2\}^{1/2}$, *and* $w_p = 1/I^{exp}(2\theta_i)$.

**Table S2.** Comparisons of the density of accessible metal sites between **FeNi-M'MOF** and other MOFs.

| MOF | Formula | Formula Weight (g mol$^{-1}$) | Density (g cm$^{-3}$) | Volumetric density of accessible metal sites (mmol cm$^{-3}$) |
|---|---|---|---|---|
| Zn-MOF-74 | $Zn_2C_8H_2O_6$ | 324.88 | 1.219 | 7.5[S3] |
| Co-MOF-74 | $Co_2C_8H_2O_6$ | 311.96 | 1.181 | 7.6[S4] |
| Ni-MOF-74 | $Ni_2C_8H_2O_6$ | 311.48 | 1.194 | 7.7[S5] |
| PCP-31 | $Cu_2C_{22}H_{12}O_{10}$ | 563.40 | 0.703 | 2.5[S6] |
| HKUST-1 | $Cu_3C_{18}H_6O_{12}$ | 604.87 | 0.879 | 4.4[S7] |
| Ni-(*m*-dobdc) | $Ni_2C_8H_2O_6$ | 311.48 | 1.200 | 7.7[S8] |
| UTSA-74a* | $Zn_2C_8H_2O_6$ | 324.88 | 1.342 | 8.3[S9] |
| **FeNi-M'MOF*** | $FeNiC_8H_4N_6$ | 298.70 | 1.375 | **9.2** (this work) |

*Noted that every open metal center in these MOFs have two accessible sites.

**Table S3.** Dual-site Langmuir fit parameters for $C_2H_2$, and $CO_2$ in **FeNi-M'MOF** at 298 K.

| | Site A | | | Site B | | |
|---|---|---|---|---|---|---|
| | $q_{A,sat}$ mol kg$^{-1}$ | $b_{A0}$ Pa$^{-1}$ | $E_A$ kJ mol$^{-1}$ | $q_{B,sat}$ mol kg$^{-1}$ | $b_{B0}$ Pa$^{-1}$ | $E_B$ kJ mol$^{-1}$ |
| $C_2H_2$ | 1 | 4.18E-13 | 40 | 4.1 | 7.70E-9 | 27 |
| $CO_2$ | 3.84 | 9.46E-10 | 25 | | | |

**Table S4.** Dual-site Langmuir fit parameters for $C_2H_2$, and $CO_2$ in **FePt-M'MOF** at 298 K.

| | Site A | | | Site B | | |
|---|---|---|---|---|---|---|
| | $q_{A,sat}$ mol kg$^{-1}$ | $b_{A0}$ Pa$^{-1}$ | $E_A$ kJ mol$^{-1}$ | $q_{B,sat}$ mol kg$^{-1}$ | $b_{B0}$ Pa$^{-1}$ | $E_B$ kJ mol$^{-1}$ |
| $C_2H_2$ | 2.3 | 1.01E-09 | 31 | 0.9 | 1.49E-11 | 30 |
| $CO_2$ | 2.8 | 2.06E-10 | 29 | | | |

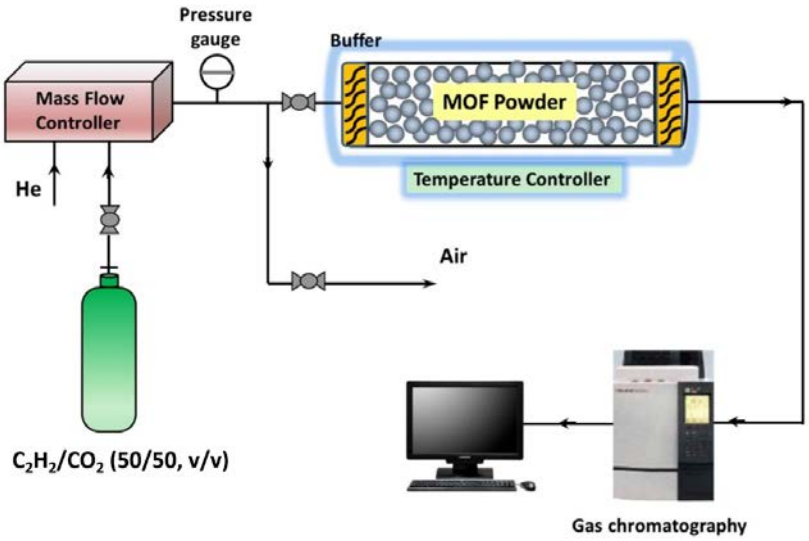


**Figure S1.** Illustration of the self-built breakthrough apparatus.

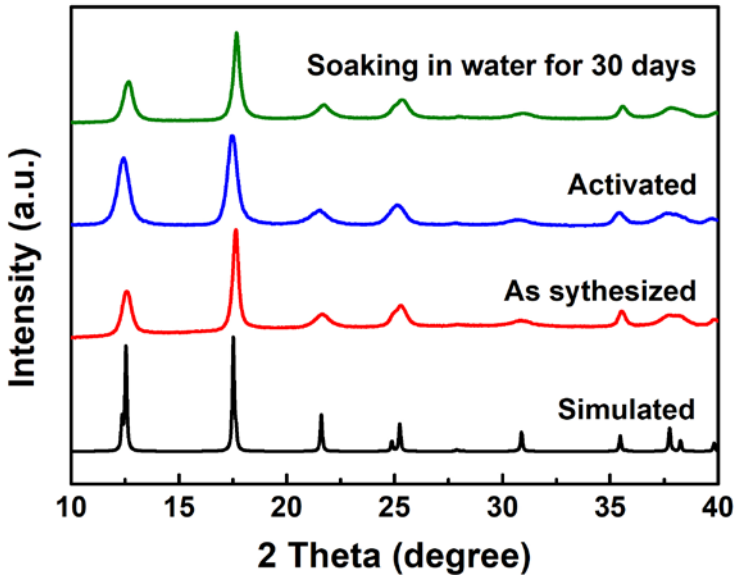


**Figure S2.** Powder X-ray diffraction patterns of FeNi-M'MOF at different conditions.

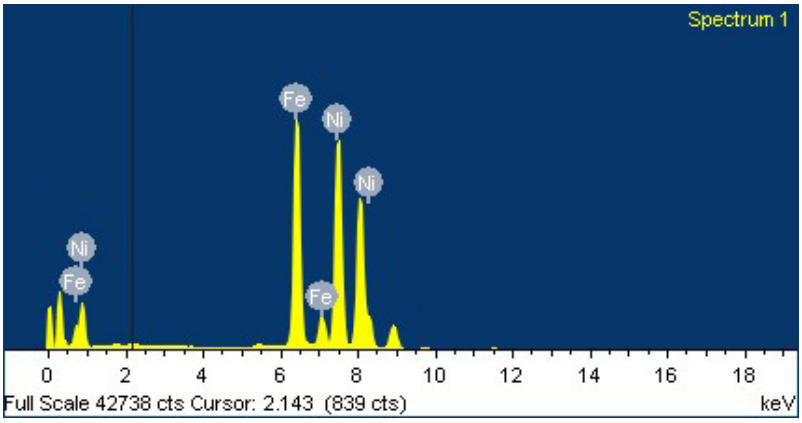


**Figure S3.** EDS spectra of **FeNi-M'MOF**. The atomic molar ratio of Fe/Ni is 1.07, which is almost identical with the theoretical ratio of 1 in **FeNi-M'MOF**.

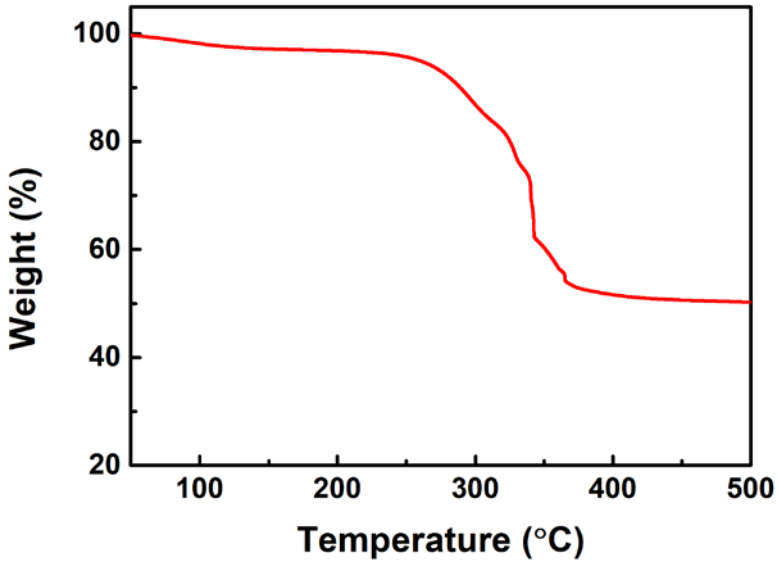


**Figure S4.** TGA curve of **FeNi-M'MOF** under air atmosphere.

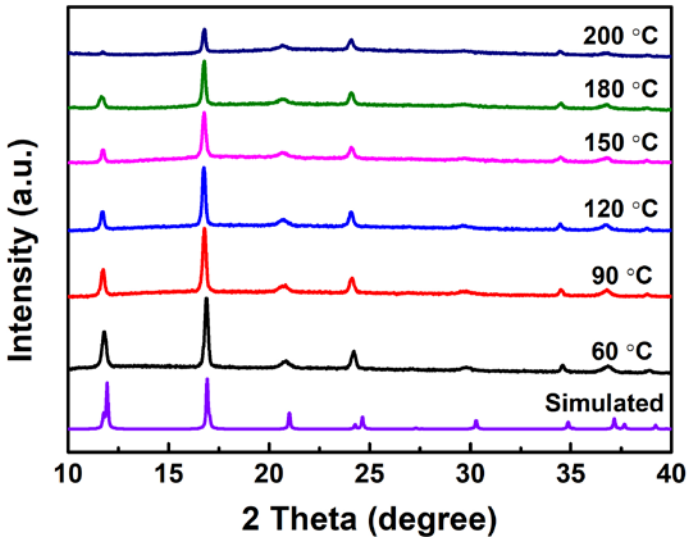


**Figure S5.** Variable-temperature PXRD patterns of FeNi-M'MOF under air atmosphere.

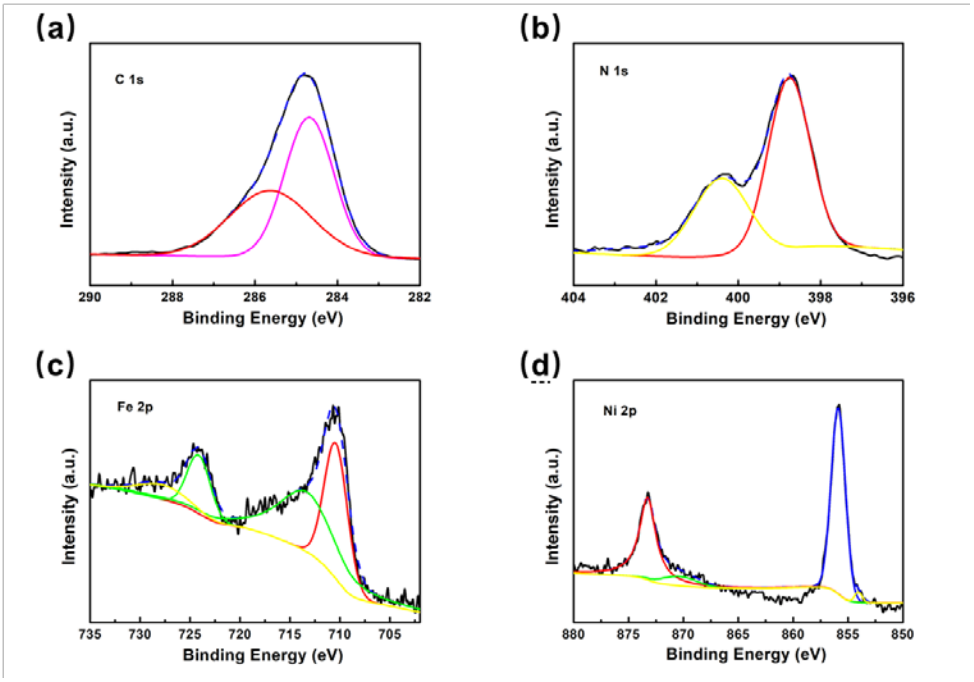


**Figure S6.** XPS spectra of **FeNi-M'MOF**. C 1s spectra (a), N 1s spectra (b), Fe 2p spectra (c) and Ni 2p spectra (d) of **FeNi-M'MOF**. The binding energies of Fe $2p_{3/2}$, $2P_{1/2}$ and satellite in **FeNi-M'MOF** are recorded at approximately 710.41 eV, 713.98 eV and 724.13 eV, which correspond to $Fe^{2+}$.[S10] The binding energies of Ni $2p_{3/2}$ and $2P_{1/2}$ in **FeNi-M'MOF** are recorded at approximately 855.8 eV and 873.28 eV, which correspond to $Ni^{2+}$.[S11] The molar ratio of Fe/Ni in **FeNi-M'MOF** is 1.03 based on XPS data, which is almost identical with the theoretical ratio of 1.

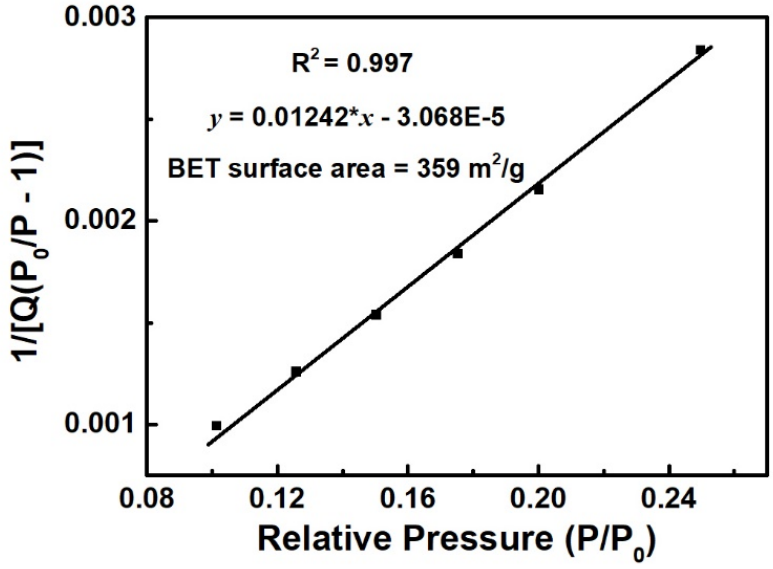


**Figure S7.** Calculation of BET surface area for **FeNi-M'MOF** based on $N_2$ adsorption isotherm at 77 K.

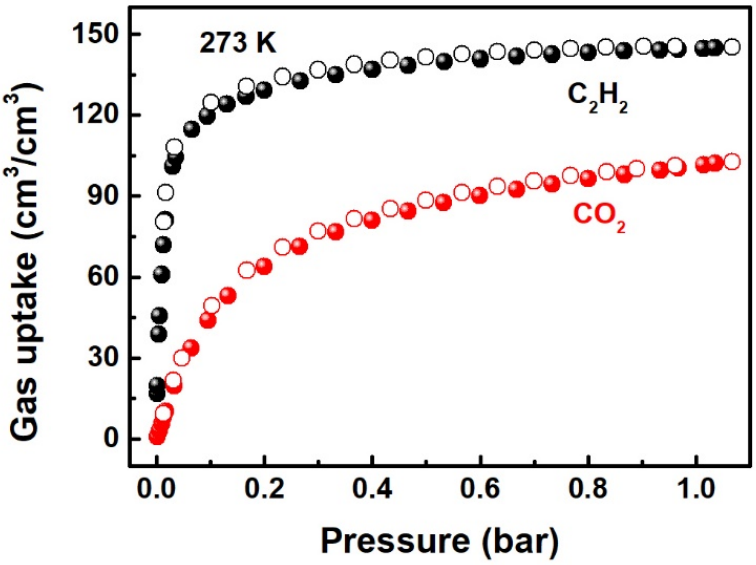


**Figure S8.** Single-component adsorption (solid) and desorption (open) isotherms of $C_2H_2$ and $CO_2$ in **FeNi-M'MOF** at 273 K.

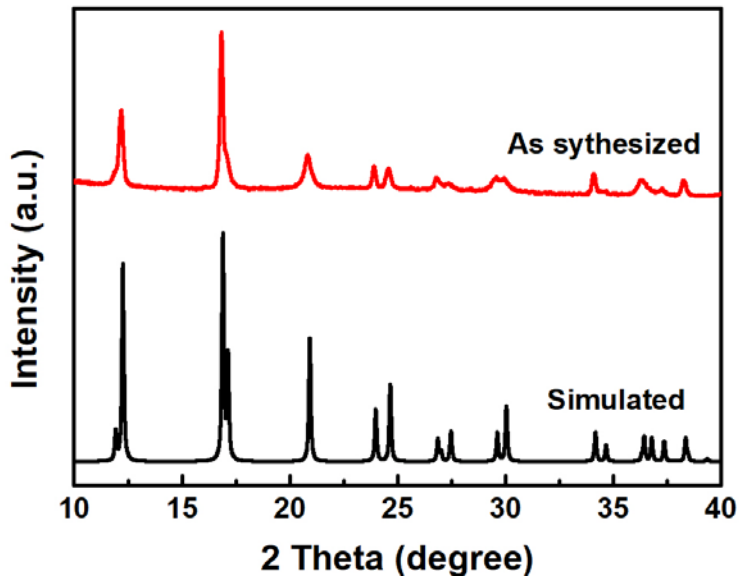


**Figure S9.** PXRD of simulated **FePt-M'MOF** and as synthesized **FePt-M'MOF**.

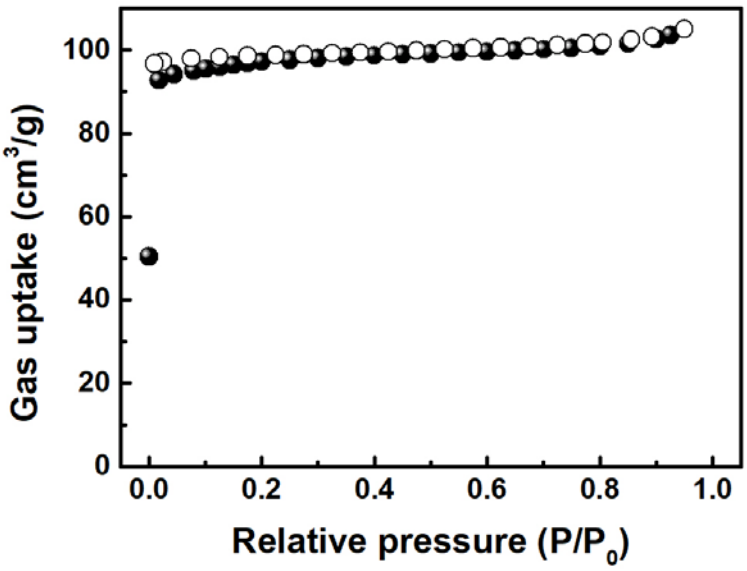


**Figure S10.** $N_2$ sorption isotherms for **FePt-M'MOF** at 77 K.

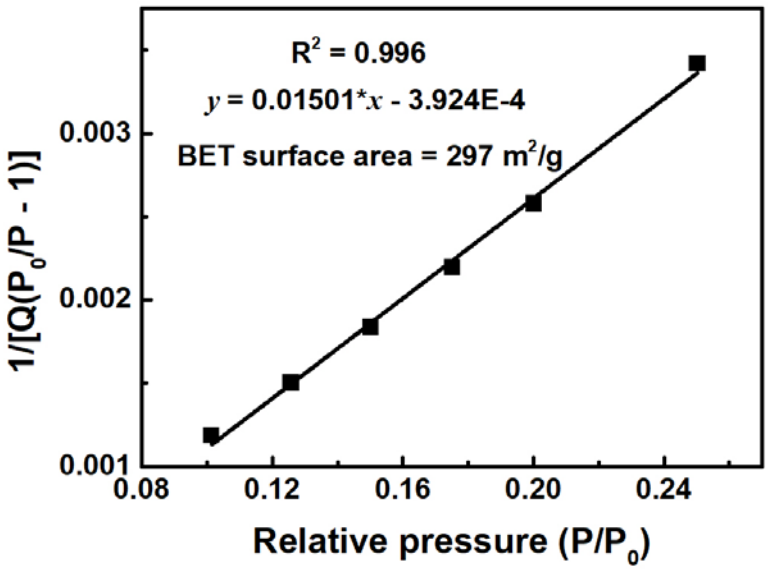


**Figure S11.** Calculation of BET surface area for **FePt-M'MOF** based on $N_2$ adsorption isotherm at 77 K.

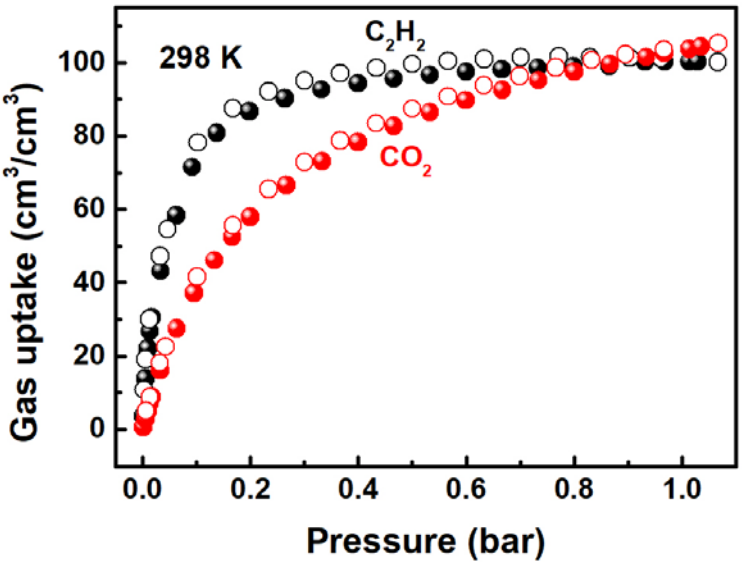


**Figure S12.** Single-component adsorption (solid) and desorption (open) isotherms of $C_2H_2$ and $CO_2$ in **FePt-M'MOF** at 298 K.

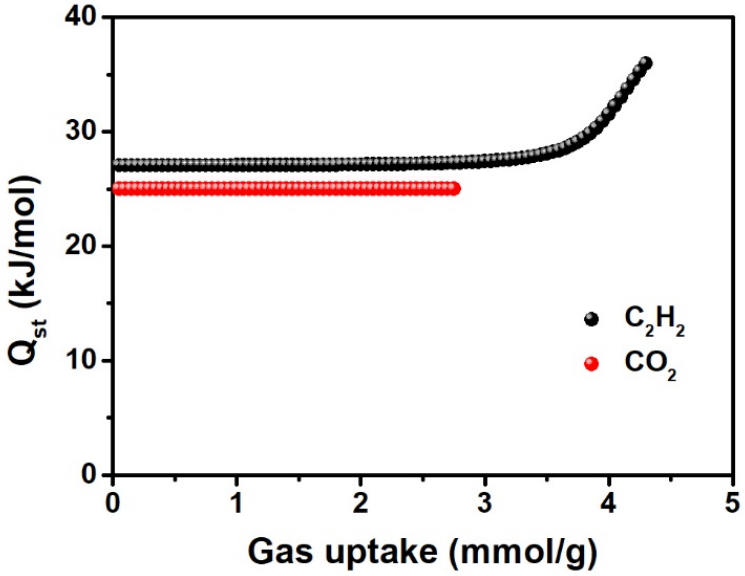


**Figure S13.** Heats of adsorption of both $C_2H_2$ and $CO_2$ in **FeNi-M'MOF**.

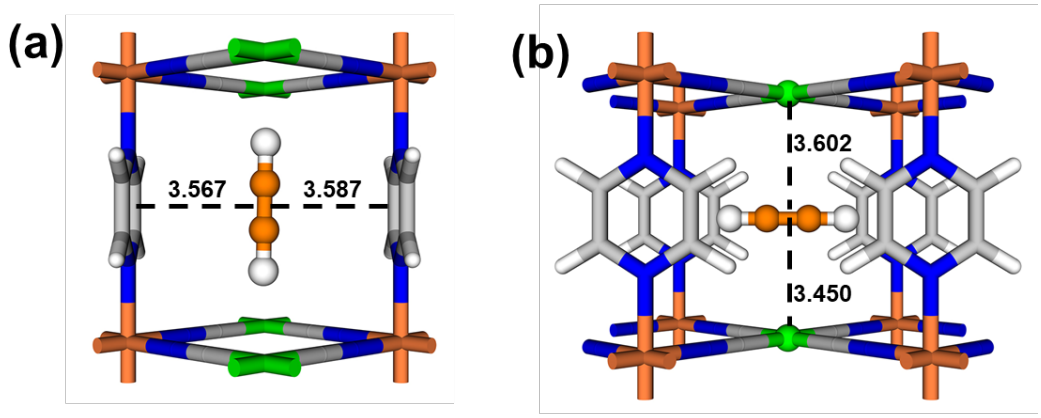


**Figure S14.** The DFT-D calculations binding sites of $C_2H_2$ in **FeNi-M'MOF**. Viewed from a/b axis (a) of site I, viewed from a/b axis (b) of site II of $C_2H_2$. The calculated $C_2H_2$ static binding energies are 41.4 kJ $mol^{-1}$ on site I and 29.9 kJ $mol^{-1}$ on site II. Fe, Ni, C, N, H in **FeNi-M'MOF** are represented by orange, green, gray, blue and white, respectively; C and H in $C_2H_2$ are represented by orange and white, respectively. The unit of the distance is Å.

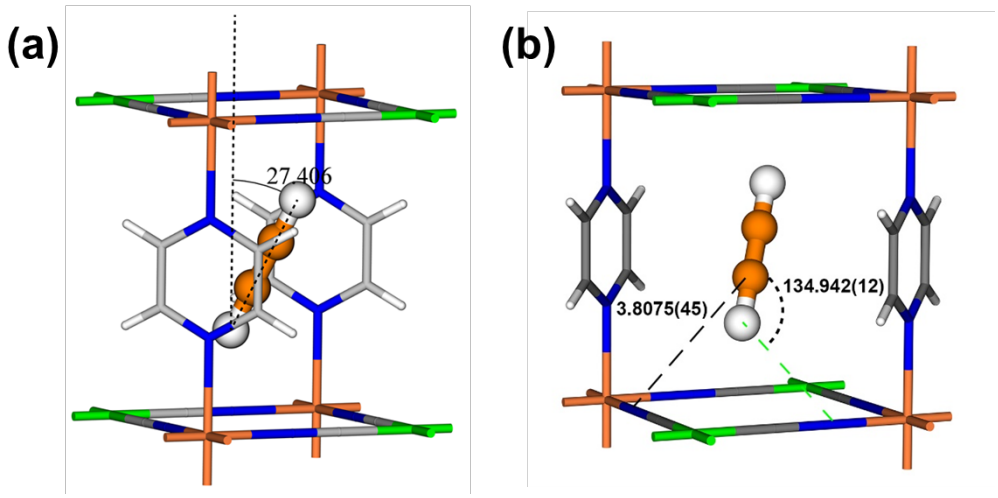


**Figure S15.** The $C^{\delta-}\cdots N^{\delta-}$ distances and bond angle of the $C\text{-}D^{\delta+}\cdots N^{\delta-}$ between $C_2D_2$ and **FeNi-M'MOF**. Fe, Ni, C, N, H in **FeNi-M'MOF** are represented by orange, green, gray, blue and white, respectively; C and D in $C_2D_2$ are represented by orange and white, respectively. The unit of the distance is Å.

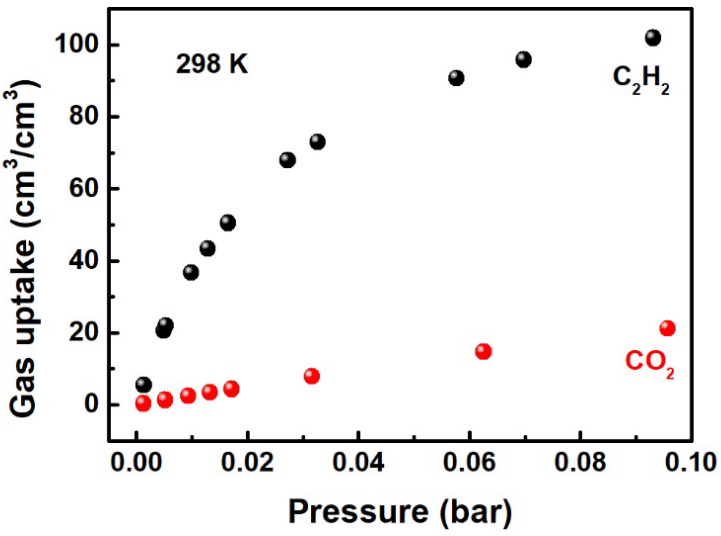


**Figure S16.** $C_2H_2$ and $CO_2$ single-component adsorption isotherms for **FeNi-M'MOF** at 298 K under low pressure (0~0.1 bar).

# References

[S1] a) R. Krishna, *RSC Adv.* **2017**, *7*, 35724-35737; b) R. Krishna, *RSC Adv.* **2015**, *5*, 52269-52295.

[S2] P. Li, Y. He, Y. Zhao, L. Weng, H. Wang, R. Krishna, H. Wu, W. Zhou, M. O'Keeffe, Y. Han, B. Chen, *Angew. Chem. Int. Ed.* **2015**, *54*, 574-577.

[S3] N. L. Rosi, J. Kim, M. Eddaoudi, B. Chen, M. O'Keeffe, O. M. Yaghi, *J. Am. Chem. Soc.* **2005**, *127*, 1504-1518.

[S4] P. D. C. Dietzel, Y. Morita, R. Blom, H. Fjellvåg, *Angew. Chem. Int. Ed.* **2005**, *44*, 6354-6358.

[S5] P. D. C. Dietzel, B. Panella, M. Hirscher, R. Blom, H. Fjellvåg, *Chem. Commun.* **2006**, 959-961.

[S6] J. Duan, M. Higuchi, J. Zheng, S.-i. Noro, I. Y. Chang, K. Hyeon-Deuk, S. Mathew, S. Kusaka, E. Sivaniah, R. Matsuda, S. Sakaki, S. Kitagawa, *J. Am. Chem. Soc.* **2017**, *139*, 11576-11583.

[S7] S. S. Y. Chui, S. M. F. Lo, J. P. H. Charmant, A. G. Orpen, I. D. Williams, *Science* **1999**, *283*, 1148-1150.

[S8] M. T. Kapelewski, S. J. Geier, M. R. Hudson, D. Stück, J. A. Mason, J. N. Nelson, D. J. Xiao, Z. Hulvey, E. Gilmour, S. A. FitzGerald, M. Head-Gordon, C. M. Brown, J. R. Long, *J. Am. Chem. Soc.* **2014**, *136*, 12119-12129.

[S9] F. Luo, C. Yan, L. Dang, R. Krishna, W. Zhou, H. Wu, X. Dong, Y. Han, T.-L. Hu, M. O'Keeffe, L. Wang, M. Luo, R.-B. Lin, B. Chen, *J. Am. Chem. Soc.* **2016**, *138*, 5678-5684.

[S10] T. Yamashita, P. Hayes, *Appl. Surf. Sci.* **2008**, *254*, 2441-2449.

[S11] D. Yan, C. Yu, D. Li, X. Zhang, J. Li, T. Lu, L. Pan, *J. Mater. Chem. A* **2016**, *4*, 11077-11085.